

Light scattering of semitransparent sintered polytetrafluoroethylene films

Qinghe Li*

Bong Jae Lee[†]

Zhuomin M. Zhang

Georgia Institute of Technology
George W. Woodruff School
of Mechanical Engineering
Atlanta, Georgia 30332

David W. Allen

National Institute of Standards and Technology
Optical Technology Division
Gaithersburg, Maryland 20899

Abstract. Polytetrafluoroethylene (PTFE) is a strongly scattering material and has been regarded to have optical properties similar to biological tissues. In the present study, the bidirectional reflectance distribution function (BRDF) and the bidirectional transmittance distribution function (BTDF) of several PTFE films, with thicknesses from 0.11 to 10 mm, are measured using a laser scatterometer at the wavelength of 635 nm. The directional-hemispherical reflectance (R) and transmittance (T) were obtained by integrating BRDF and BTDF for normal incidence. Comparison of the ratio of the measured R and T with that calculated from the adding-doubling method allows the determination of the reduced scattering coefficient. Furthermore, the effect of surface scattering is investigated by measuring the polarization-dependent BRDF and BTDF at oblique incidence. By analyzing the measurement uncertainty of BTDF in the near-normal observation angles at normal incidence, the present authors found that the scattering coefficient of PTFE should exceed 1200 cm^{-1} , which is much greater than that of biological tissues. On the other hand, the absorption coefficient of PTFE must be less than 0.01 cm^{-1} , much smaller than that of biological tissues, a necessary condition to achieve $R \geq 0.98$ with a 10-mm-thick slab. © 2008 Society of Photo-Optical Instrumentation Engineers. [DOI: 10.1117/1.2992485]

Keywords: bidirectional reflectance distribution function; bidirectional transmittance distribution function; polytetrafluoroethylene; radiative transfer; semitransparent; volume scattering.

Paper 08083RR received Mar. 6, 2008; revised manuscript received Jun. 11, 2008; accepted for publication Aug. 11, 2008; published online Oct. 6, 2008.

1 Introduction

Polytetrafluoroethylene (PTFE) is known as a strongly scattering and diffusely reflecting material. The diffuse reflection is mainly due to the volume scattering of light inside the material. When the light enters a volume-scattering material, it is scattered by microstructures and propagates in random directions before escaping the medium. Due to its characteristics of being a nearly diffuse reflector, PTFE has been used as a diffuse-reflectance standard in the spectral range from 200 to 2500 nm by the National Institute of Standards and Technology (NIST),¹ as a calibration standard for onboard sensors on satellites in remote sensing,^{2–5} as whiteness standards in colorimetry,^{6,7} and as a coating layer in integrating spheres.⁸ In addition, since both PTFE and most biological tissues are strongly scattering materials, researchers have used PTFE as tissue phantoms to simulate layers of skin for the study of burn depth.⁹

Light scattering in a turbid medium such as PTFE and tissue has been studied extensively. The angle-resolved scattering of a turbid medium could not be predicted until the

more general radiative transfer equation (RTE) was developed.¹⁰ The common techniques for solving RTE include Chandrasekhar's X and Y functions,¹⁰ the discrete-ordinates method,¹¹ the Monte Carlo method,^{12–15} and the adding-doubling method.¹⁶ To describe light propagation in a PTFE slab using the RTE, the scattering coefficient (σ_s), absorption coefficient (a_s), and the scattering phase function need to be known. The determination of these parameters typically requires several measurements, among which are:¹⁷ 1. directional-hemispherical reflectance (R); 2. directional-hemispherical transmittance (T); 3. absorptance (A); 4. collimated light transmittance (T_d); and 5. angular distribution of scattered light from a sample thin enough to ensure that only single scattering occurs. The double-integrating-sphere method has been widely used for measuring R and T .^{18,19} With the additional measurement of T_d , these parameters can be determined with an inverse method.^{20,21}

Using an approach similar to the double-integrating-sphere method, Huber, Heitz, and Bauerle²² reported the scattering coefficient, absorption coefficient, and the asymmetric parameter in the Henyey–Greenstein phase function of PTFE films with thicknesses from 190 to 845 μm . The scattering parameters of PTFE reported in their study are very similar to those of biological tissues.¹⁷ For example, the scattering and absorp-

*Current address: Cummins Fuel Systems, Cummins Inc., Columbus, IN 47201.

[†]Current address: Department of Mechanical Engineering and Materials Science, University of Pittsburgh, Pittsburgh, PA 15261.
Address all correspondence to: Zhuomin M. Zhang, George W. Woodruff School of Mechanical Engineering, Georgia Institute of Technology, Atlanta, Georgia; E-mail: zhuomin.zhang@me.gatech.edu.

Table 1 Parameters of the PTFE samples and the directional-hemispherical reflectance and transmittance obtained by integrating the measured BRDF and BTDF at $\lambda=635$ nm.

Sample	Thickness d (mm)	Density ρ (g/cm ³)	Reflectance R	Transmittance T	$R+T$	R/T
1	0.109±0.003	1.65±0.05	0.558	0.425	0.983	1.31
2	0.259±0.003	1.82±0.05	0.723	0.282	1.005	2.56
3	0.522±0.004	1.90±0.05	0.822	0.179	1.001	4.58
4	1.057±0.008	1.70±0.05	0.921	0.090	1.010	10.4
5	10.1±0.1	1.52±0.05	0.988	—	—	—

tion coefficients at 633 nm were $\sigma_\lambda=240$ cm⁻¹ and $a_\lambda=3.6$ cm⁻¹, respectively. However, it appears that these authors did not distinguish the scattered light in the parallel direction from the collimated light transmission. For PTFE samples with thicknesses greater than 190 μ m, the scattered light would dominate the transmittance even in the direction parallel to the incident light; in other words, since T_d is essentially zero, the collimated light does not contribute to the detector signal. Unless the PTFE films can be made thinner than approximately four times the mean free path of the incident light, it is not feasible to unambiguously determine the scattering coefficient because the collimated light would be much weaker than the forward scattered light. This difficulty also applies to the determination of scattering phase function by measuring the angular distribution of scattered light from a sample because the single scattering condition cannot be guaranteed. Furthermore, the measurement of absorptance of PTFE using an integrating sphere is problematic because the absorption coefficient of this material is so small that the uncertainty of integrating sphere measurements often makes the absorptance imperceptible.

In the present study, the bidirectional reflectance distribution function (BRDF) and bidirectional transmittance distribution function (BTDF) of five PTFE films, whose thicknesses vary from 0.11 to 10 mm, were measured using a laser scatterometer at 635 nm. Integrating the measured BRDF and BTDF over the corresponding hemisphere yields the R and T for normal incidence. The reduced scattering coefficient $\sigma'_\lambda=\sigma_\lambda(1-g)$, where g is the asymmetric parameter in the Henyey–Greenstein phase function, was determined by fitting R/T (i.e., the ratio of R and T) of the thin-film samples with those calculated from the adding-doubling method. The ranges of σ_λ , g , and a_λ were also estimated by analyzing the measurement results. The polarization-dependent BRDF and BTDF were measured at oblique incidence to demonstrate the effect of surface scattering. Moreover, a monochromator and an integrating sphere were employed to measure R and T in the wavelength region from 350 to 1050 nm.

2 Method

2.1 Bidirectional Measurements

The five sintered Zenith PTFE samples were purchased from SphereOptics (Concord, New Hampshire). The thicknesses of

samples 1 to 5 were measured with a micrometer to be (0.109 ± 0.003), (0.259 ± 0.003), (0.522 ± 0.004), (1.057 ± 0.008), and (10.1 ± 0.1) mm, respectively. Table 1 lists the sample parameters as well as some of the measured optical properties. The densities of samples range from 1.5 to 1.9 g/cm³. These samples were cut into 50 × 50-mm² pieces from a sheet, except for sample 5, which came as a 50 × 50-mm² piece from the manufacturer.

A three-axis automated scatterometer (TAAS)²³ with a 635-nm laser diode was used for the measurement of the BRDF and BTDF. The BRDF is defined as the reflected radiance divided by the incident irradiance,

$$f_r = \frac{dI_r}{I_i \cos \theta_i d\Omega_i}, \quad (1)$$

where I_r is the reflected radiance, I_i is the incident radiance, θ_i is the angle of incidence, and $d\Omega_i$ is the solid angle of the incident light. The measurement equation of BRDF is given as

$$f_r = C_I \frac{P_o}{P_i \cos \theta_o \delta\Omega_o}, \quad (2)$$

where P_i and P_o are respectively the incident and reflected optical powers reaching the detector, θ_o is the observation angle (i.e., polar angle of the detector), and $\delta\Omega_o$ is the solid angle of the detector. An instrument calibration factor C_I is introduced and is determined later. The BTDF is defined in a similar way by replacing I_r with I_t (i.e., transmitted radiance) in Eq. (1). A collimation lens was placed in front of the laser diode, resulting in a highly collimated light with a beam divergence less than 0.0126 deg. A lock-in amplifier was used to produce a modulated voltage signal for the laser diode controller; thus the effect of stray light can be minimized. The samples were mounted in a rotary stage so that the incidence angle θ_i could be changed. A detector controlled by another rotary stage measured the scattered light in an observation angle θ_o ranging from -90 to 90 deg. In front of the detector, there was a precision aperture with a diameter of 8 mm. The distance between the aperture and the sample holder was measured to be (522.5 ± 0.5) mm. Consequently, the detector solid angle was 1.84×10^{-4} sr and the half cone angle was approximately 0.45 deg. Since the detector blocked the inci-

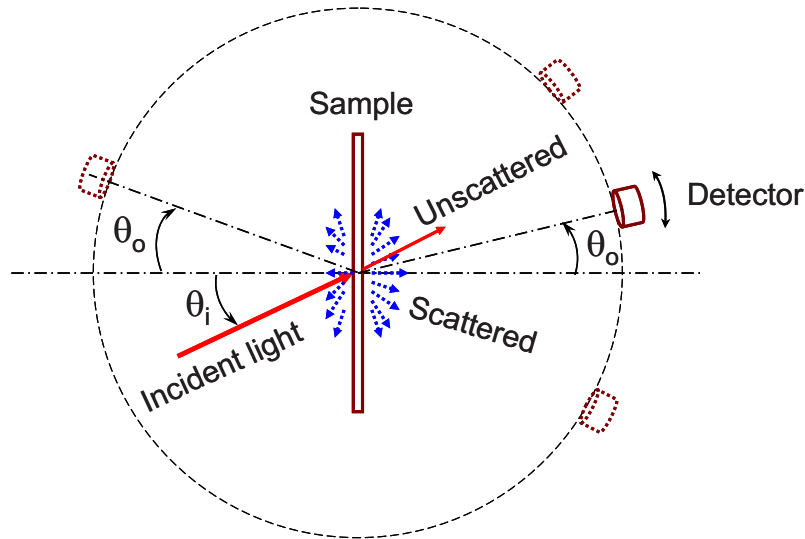


Fig. 1 Schematic of volume scattering by a slab and the laser scatterometer. The unscattered light is the transmitted collimated beam. The observation angle θ_o is relative to the surface normal of the sample and defined separately for BRDF and BTDF measurements. In the experiments, the direction of the laser is fixed. The sample can be rotated to change the incidence angle θ_i , and the detector can be rotated around the sample.

dent light, the BRDF within ± 3 deg of the retroreflection direction could not be measured.²³

Figure 1 shows the schematic of light scattering from a semitransparent film. The observation angle is defined separately for BRDF and BTDF as depicted in the figure. For BTDF measurement when $\theta_o = \theta_i$, both the transmitted collimated light (i.e., unscattered light) and the scattered light may contribute to the detector signal. The measured BTDF should exhibit a noticeable peak at $\theta_o = \theta_i$ when the collimated light transmittance is significant enough.

2.2 Spectral Characterization

The wavelength dependence of R and T was characterized with a monochromator and an integrating sphere at wavelengths from 350 to 1050 nm.²⁴ The light source was a tungsten-halogen lamp. The rotation of two gratings inside the monochromator and the change of filters at the inlet of the monochromator are capable of achieving a wavelength resolution of 10 nm. The rms fluctuation of power from the monochromator was estimated to be 1%. The light exiting the monochromator is directed to the sample mounted either before the sphere entrance port for measuring T or at the back of the sphere wall for measuring R . A chopper is used to obtain a phase-locked optical signal. A silicon detector was located at the bottom port with a baffle to prevent the direct illumination of the detector from the scattered light. The detector output is amplified by a transimpedance preamplifier before being sent to a lock-in amplifier. The integrating sphere has an inner wall of 200 mm in diameter. The entrance port is 25 mm in diameter. The inner wall is coated with PTFE with a reflectance between 0.98 and 0.99 in the visible spectral range.

2.3 Theory and Calculations

With the assumptions that the medium does not emit light (i.e., cold medium), the wave-like interactions are negligible,

the medium is homogeneous, and the polarization state is neglected, the light scattering in a PTFE film can be modeled using the RTE as

$$\frac{1}{\sigma_\lambda + a_\lambda} \frac{dI_\lambda(\hat{s})}{ds} = -I_\lambda(\hat{s}) + \frac{\omega_\lambda}{4\pi} \int_{4\pi} I_\lambda(\hat{s}_i) \Phi(\hat{s}_i, \hat{s}) d\Omega_i, \quad (3)$$

where I_λ is the (spectral) radiance, s is the physical distance that the light travels, $\omega_\lambda = \sigma_\lambda / (\sigma_\lambda + a_\lambda)$ defines the scattering albedo, \hat{s} and \hat{s}_i represent the light propagation directions, Ω_i is the solid angle, and Φ is the scattering phase function. In many applications, the Henyey–Greenstein function is used as the scattering phase function and is given by²⁰

$$\Phi_{\text{HG}}(\cos \Theta) = \frac{1 - g^2}{(1 + g^2 - 2g \cos \Theta)^{3/2}}, \quad (4)$$

where the scattering angle Θ is the angle between the propagation directions of the incident light and the scattered light (i.e., $\cos \Theta = \hat{s}_i \cdot \hat{s}$), and g is called the asymmetric parameter (ranging from -1 to 1). The Henyey–Greenstein function yields isotropic scattering when $g=0$. If $g > 0$, there are more forward scattered photons than backward scattered photons. If g approaches 1 , all photons are scattered in the direction parallel to the incident light. However, if $g < 0$, more photons are scattered backward than forward. If g approaches -1 , all photons will be scattered in the opposite direction of the incident light. The RTE governs the changes of radiance along an infinitesimal distance inside the medium. As a beam of light travels a distance ds in the medium, the radiance is attenuated due to scattering and absorption. Conversely, the radiance is enhanced by the incoming light scattered from other directions. Due to the complexity of the integrodifferential equation, no effective method is available that can analytically solve the RTE without some sort of approximation.

If only the hemispherical properties are of interest, the adding-doubling method is an effective technique that results in high accuracy for obtaining R and T of an absorbing and scattering medium. The adding-doubling method was introduced by van de Hulst²⁵ to solve the RTE in a parallel slab composed of multiple layers. In the adding method, if the reflection and transmission functions of each individual layer are known, the reflection and transmission functions of the composite can be calculated. The adding method is termed as the doubling method when the layers are identical in thickness and in all the RTE parameters.²⁰ The reflection and transmission functions for an arbitrarily thick slab can be obtained by repeatedly adding and doubling the layers until the desired thickness is reached. Subsequently, the directional-hemispherical reflectance and transmittance can be calculated by integrating the reflection and transmission functions. Detailed discussion of the adding-doubling method can be found from Refs. 16 and 20. The adding-doubling method requires inputs of the scattering albedo, optical thickness $\tau_\lambda = (\sigma_\lambda + a_\lambda)d$ with d being the film thickness, and the asymmetric parameter g to predict the directional-hemispherical properties of PTFE films.

A Monte Carlo algorithm was developed to model the BRDF and BTDF by considering volume scattering but neglecting the effect of surface scattering. Furthermore, the Monte Carlo simulation does not consider the dependent multiple scattering and coherent wave-like interactions. After a photon bundle is released from air to the PTFE medium, the propagation step between subsequent scattering events is calculated by $l = -\ln(R_1)/(\sigma_\lambda + a_\lambda)$, where R_1 is a random number between 0 and 1 and is generated based on a quasirandom sequence.²⁶ The previous equation results in the mean free path (i.e., average propagation step) of $1/(\sigma_\lambda + a_\lambda)$. The angle between the direction vectors before and after the scattering is determined by the Henyey–Greenstein scattering phase function given in Eq. (4) following the procedure described by Wang, Jacques, and Zheng.²⁷ After each scattering event, the energy of the photon bundle reduces to $\omega_\lambda E$ due to the absorption, where E is the energy of the photon bundle before scattering.

In the Monte Carlo simulation, R is calculated as the summation of the reflected photon bundle energy divided by the total energy of the incident photon bundle, which is the product of the number of photon bundles and the energy assigned to each incident photon bundle. Similarly, T is calculated as the summation of the transmitted photon bundle energy divided by the total energy of the incident photon bundles. The calculated R and T using the Monte Carlo simulation with a photon bundle number of 1×10^6 is in agreement with that using the adding-doubling method within a statistical fluctuation of 0.5%. To determine the BRDF and BTDF, a virtual detector with a solid angle of 1.76×10^{-3} sr is placed in 5-deg intervals in the corresponding hemisphere. For the calculation of BRDF and BTDF, 2×10^7 photon bundles are used and each run takes approximately 2.5 h of CPU time with a 3.2-GHz Pentium 4 processor when the thickness of the sample is 0.1 mm. The resulting fluctuation is within 1.5% of the BRDF and BTDF values. Additional photon bundles can be used to reduce the statistical fluctuation with longer calculation time.

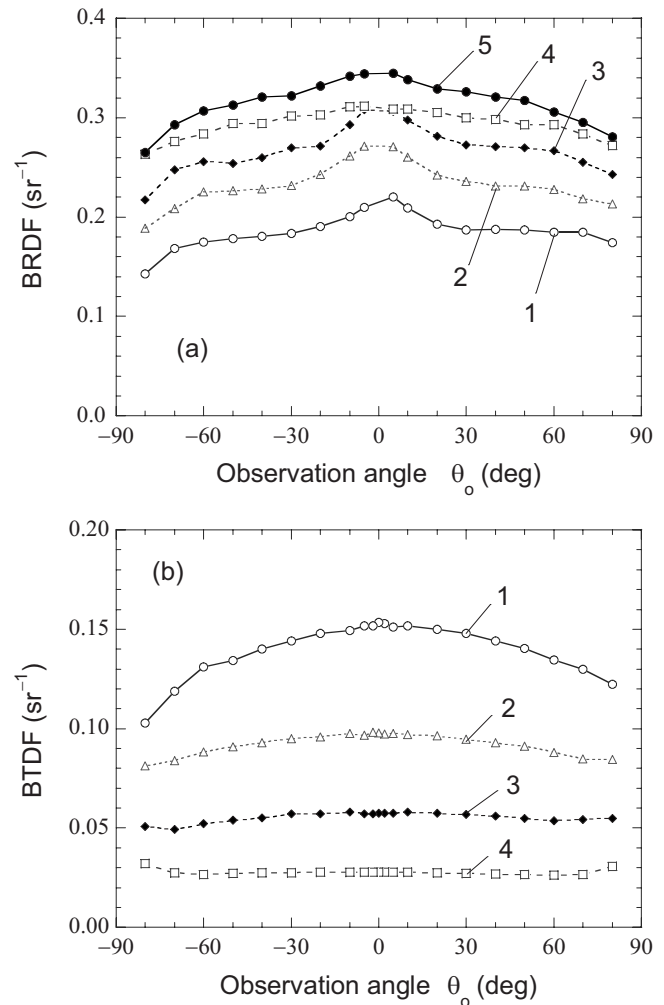


Fig. 2 Measured (a) BRDF and (b) BTDF, averaged over the two polarizations, at normal incidence for $\lambda = 635$ nm.

3 Results

3.1 Measured Bidirectional Reflectance Distribution Function and Bidirectional Transmittance Distribution Function

Figure 2 shows the measured BRDF for all five samples and the BTDF for samples 1 to 4 for normal incidence at the wavelength $\lambda = 635$ nm. The transmittance of sample 5 is less than 0.01, and its BTDF cannot be measured due to the limited signal-to-noise ratio. The measured BRDF and BTDF exhibit nearly diffuse characteristics. For a perfectly diffuse reflector, the BRDF should be a constant of 0.318 sr^{-1} . In a round-robin test of the PTFE material, Early et al.²⁸ also reported the similar variation of the BRDF of thick PTFE slabs. As the sample thickness decreases, the corresponding BRDF value decreases because of the increased transmission. Interestingly, the hump in the BRDF near $\theta_o = 0$ deg becomes more obvious as the thickness decreases. Due to the measurement uncertainty of the laser scatterometer, the measured BRDF does not exhibit perfect symmetry with respect to $\theta_o = 0$ deg.

As expected, the BTDF values increase as the sample thickness decreases. The measurements reveal that the BTDF

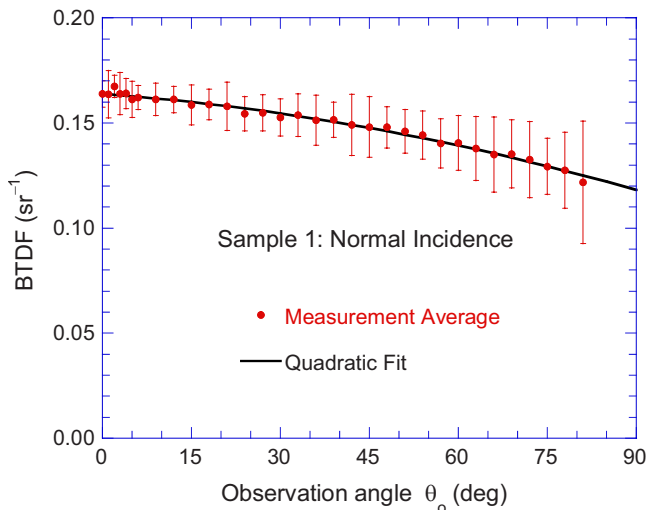


Fig. 3 Average of eight BTDF measurements for sample 1 and the fitted polynomial curve. The error bars show the measurement uncertainty with 95% confidence interval.

of samples 2, 3, and 4 are flatter than the corresponding BRDF even though the values are smaller. This can be explained by the multiple scattering of light inside the film. In order for the photon bundles to transmit through the PTFE films, they need to experience numerous scattering events, resulting in random propagation in the medium. Therefore, the BTDF of sample 4 with thickness of 1 mm is nearly uniform within ± 75 deg observation angles.

To obtain the hemispherical properties, the BRDF and BTDF data need to be carefully analyzed and fitted to perform integration. Additional measurements with closely spaced data intervals were performed. As an example, Fig. 3 shows the average of the measured BTDF (circles) and the fitted (solid line) BTDF of sample 1 at normal incidence. Eight measurements were conducted at different locations on the sample. The location on the sample was changed by rotating it by 45 deg after each measurement. Because the laser beam was not aligned to the center of rotation of the sample, the location of the laser spot changed when the sample was rotated. Error bars stand for the random uncertainty at the 95% confidence level. The measured results beyond 78 deg are not reliable because of the alignment difficulty. Since the measurement exhibits some fluctuations due to the measurement uncertainty and sample inhomogeneity, a polynomial equation was used to fit the BTDF data. For BTDF of sample 1, a quadratic function is sufficient. The standard error of estimate of the fitted equation is 0.0015 sr^{-1} , which is much smaller than the standard deviation of the data points. Notice that an extrapolation of the fitted equation for θ_o from 78 to 90 deg is performed before the integration; however, the relative error caused by this extrapolation is estimated to be less than 0.5%. In addition, the bidirectional properties are assumed to be symmetric with respect to $\theta_o=0$ deg.

The polynomial fitting functions are integrated to obtain R from the BRDF and T from the BTDF of each sample. When C_I is taken as 1, the summation of R and T is always greater than unity by approximately 6%. While the measurements of TAAS agree well with specular samples (within 2% for a

smooth Si), it is about 5% higher for a rough silicon surface and about 5% higher for the 10-mm-thick PTFE than those obtained from a standard reference instrument at NIST.^{23,28} This may be caused by the detector collection geometry and the uncertainty of the aperture area. To reduce the bias uncertainty, all TAAS measurement results are reduced by 6%. This may be considered as a self-calibration procedure. With $C_I=0.943$, the reflectance of sample 5 obtained by integration of BRDF is 0.988, which agrees well with the reported values.⁸ The summation of R and T for each of the thinner samples is about unity, as shown in Table 1. When the sample location is fixed, the variation of repeated BRDF and BTDF measurements is within 2%. The combined uncertainty of TAAS is within 5% with a confidence level of 95%. For BTDF of sample 1, however, the data variation at different locations on the sample is greater than the instrument uncertainty due to sample inhomogeneity.

The effects of incidence angle on the BRDF are shown in Fig. 4 for all samples. The measurements were performed at incidence angle $\theta_i=0, 30, 50,$ and 70 deg with a linear polarizer. The results are plotted in terms of $\text{BRDF}^* \cos(\theta_o)$ to make the comparison easier. Even at oblique incidence, the diffuse scattering feature is preserved in a large observation angle range except a peak in the forward scattering direction. The peak is much higher for s -polarization than for p -polarization, suggesting that surface scattering becomes important at large angles of incidence. This can be understood by two facts: 1. the surface looks smoother at glazing angles; and 2. the reflectance at the interface between air and PTFE is higher for s -polarization than for p -polarization. The Brewster angle $\theta_B=\tan^{-1}(n)$ is about 54 deg for refractive index $n=1.36$. At the Brewster angle, the surface reflectance for p -polarization approaches zero. When the data are examined more carefully, the BRDF for $\theta_i=50$ deg is higher than that for $\theta_i=30$ deg at large observation angles. Hence, volume scattering must also play a role in the enhanced forward scattering. It can also be seen that for samples 4 and 5, the peaks at $\theta_i=70$ deg and $60 \text{ deg} < \theta_o < 80 \text{ deg}$ are much lower than for samples 1 to 3. Visual observation reveals that sample 1, 2, and 3 may contain some surface crystallization that has improved the smoothness and specularly of these samples. This may be the reason for the specular peaks in samples 1 to 3 for the s -polarization at $\theta_i=30$ and 50 deg. At $\theta_i=70$ deg, samples 4 and 5 also exhibit specular peaks for s -polarization but with a smaller peak than that of the thinner samples.

The increased BRDF at oblique incidence results in a reduction in the BTDF as depicted in Fig. 5, where the ordinate is in terms of $\text{BTDF}^* \cos(\theta_o)$. It should be noted that the scale of the ordinates is different for each sample. The data points at $\theta_o=-5$ and -10 deg were missing for $\theta_i=70$ deg due to blocking of the beam by the rotary stage. As discussed earlier, the BRDF decreases with increasing thickness, and also the polarization has little effect on the BRDF at normal incidence. It can be clearly seen that more reduction of BTDF existed for s -polarization than for p -polarization. On the other hand, because the transmitted light experiences multiple scattering events, they are redirected into random directions. Hence, the BTDF shape appears symmetric about $\theta_o=0$ deg, regardless of the incidence angle.

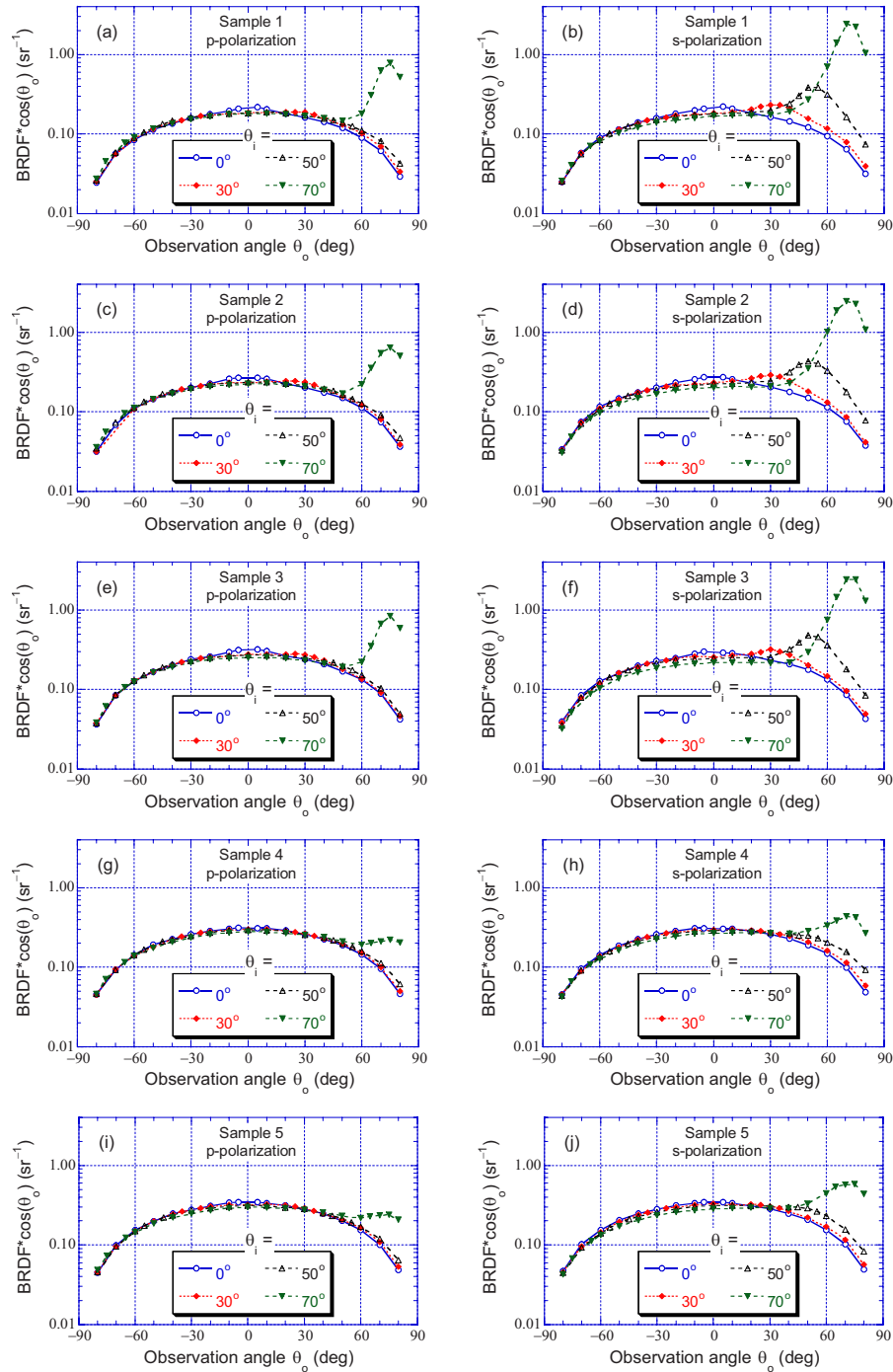


Fig. 4 BRDF of all five samples at various incidence angles for both *p*- and *s*-polarizations.

3.2 Estimation of σ'_λ and the Ranges of a_λ , σ_λ , and g

If the absorption coefficient a_λ is negligible, the directional-hemispherical properties of a volume scattering medium depend only on the film thickness d and the reduced scattering coefficient $\sigma'_\lambda = \sigma_\lambda(1-g)$.²⁰ In the present study, σ'_λ is estimated by comparison of the calculated *R*-to-*T* ratio for the given thickness with those obtained by integrating the measured BRDF and BTDF over the corresponding hemisphere. In fact, the ratio *R*/*T* is independent of the bias uncertainty in the scatterometer measurement. Note that the refractive index

of PTFE is around 1.36, and the reflectance at the interface between air and PTFE is approximately 2.3% near normal incidence. The reflected light will be distributed hemispherically due to surface roughness and may exhibit a broadened specular peak. In the present study, the adding-doubling method is employed to solve the RTE for the PTFE films, without considering surface scattering due to refractive index mismatch and surface roughness.

To determine σ'_λ , the ratio *R*/*T* is calculated as a function of σ'_λ for the thickness d equal to the thicknesses of the four

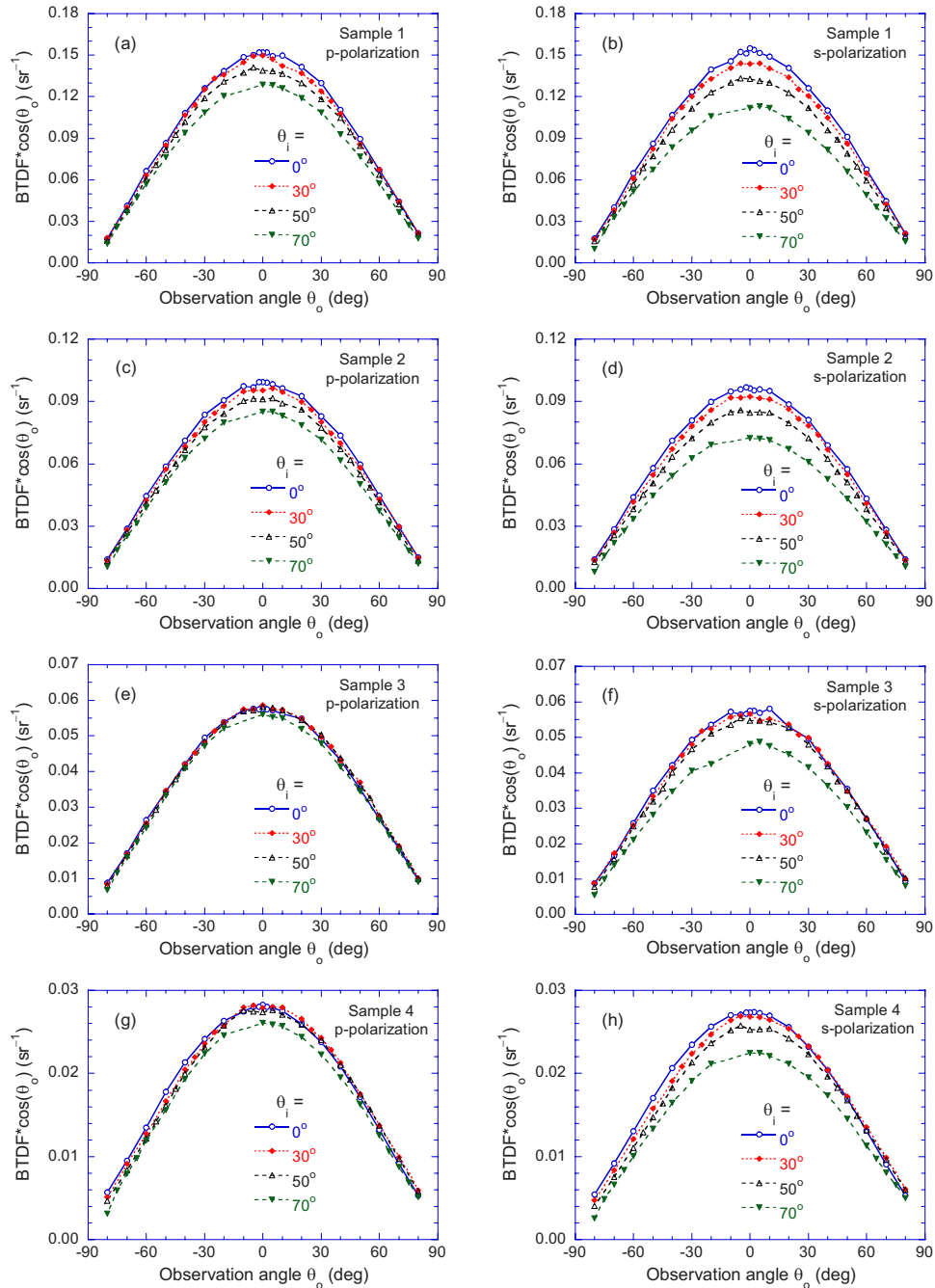


Fig. 5 BTDF of the four thin-film samples at various incidence angles for both polarizations.

thinner samples. By assuming that all samples have the same σ'_λ , the standard error of estimate between the calculated and measured R/T for all four samples is a function of σ'_λ only. The standard error of estimate between the measured and the calculated R/T values reaches a minimum at $\sigma'_\lambda = 167 \text{ cm}^{-1}$. Considering the measurement uncertainty and sample-to-sample variation, the reduced scattering coefficient is estimated to be $\sigma'_\lambda = (167 \pm 20) \text{ cm}^{-1}$. Here, the obtained σ'_λ value is approximately one order of magnitude higher than the reported value in Ref. 22.

Figure 6 shows the measured R/T ratio and the calculated values using the adding-doubling method with σ'_λ

$= 167 \text{ cm}^{-1}$. The inset shows the results for smaller d values to compare the measurement with the calculation clearly. While in general the reflectance and transmittance are complicated functions of the film thickness, the ratio R/T exhibits a linear dependence on the film thickness for d from 0.1 to 10 mm. A linear regression of the adding-doubling calculations yields that $R/T = 0.59\sigma'_\lambda d$. Using different values of σ'_λ , it was found that a constant of 0.59 remains the same, regardless of the value of σ'_λ .

For strongly scattering and nonabsorbing media, the linear dependence of R/T on $\sigma'_\lambda d$ can be derived from other approximation models such as the Kubelka–Munk model (or

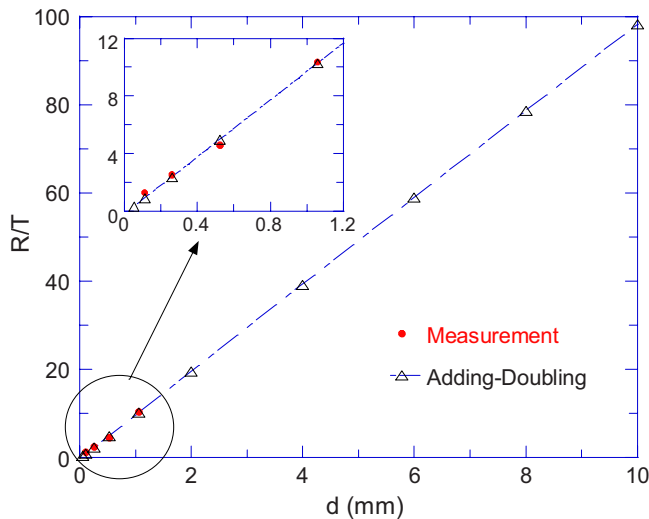


Fig. 6 The ratio of R/T obtained from the integration of measured BRDF and BTDF (dots) and that calculated using adding-doubling method (triangles), where the inset shows the results for a small d range. The parameters used for the calculation are $\sigma' = 167 \text{ cm}^{-1}$ and $g = 0.9$.

two-flux model)²⁹ and the three-flux model.³⁰ Star, Marijnissen, and van Gemert³¹ reported the transformation between the scattering coefficient used in the Kubelka–Munk model and the scattering coefficient σ_λ of RTE. By solving the governing equations of these models, it can be shown that the ratio of R/T is in linear relationship with $\sigma'_\lambda d$, similar to that calculated from the adding-doubling method. The linear dependence of R/T on film thickness for strongly scattering and nonabsorbing mediums can be obtained from all these models, including the adding-doubling method, Monte Carlo simulation, Kubelka–Munk model, and the three-flux model. Although there are some variations in the final analytical expressions, depending on different model approximations, the linear relationship provides a very simple approach for the determination of the reduced scattering coefficient of PTFE films by measuring R and T of a sample with known thickness.

Table 2 lists the calculated R and T of the 10-mm-thick PTFE slab using the adding-doubling method. The parameters are set to be $\sigma'_\lambda = 167 \text{ cm}^{-1}$ and $g = 0.9$ (i.e., $\sigma_\lambda = 1670 \text{ cm}^{-1}$). As mentioned in the previous section, the reduced scattering coefficient is the dominant factor in determining the hemispherical properties. Hence, the calculation shown in Table 2 is also applicable for different g values as long as σ'_λ is fixed. The absorption coefficient must be less than 0.01 cm^{-1} for R of the 10-mm-thick sample to be greater than 0.977. It should be noted that the measured values are usually greater than 0.98.⁸

As can be seen from Table 2, the adding-doubling calculation suggests that the 10-mm-thick slab can have a nonzero transmittance as large as 0.01 when the absorption is neglected. To assess the transmittance value, the integrating sphere is used with the 635-nm laser diode as the light source. The sample is placed at the entrance port. The transmittance of sample 5 (10.1 mm thick) is estimated to be 0.007 ± 0.002 , which indicates that the absorption coefficient

Table 2 The influence of the absorption coefficient on the directional-hemispherical reflectance and transmittance of the 10-mm-thick PTFE slab when $\sigma_\lambda = 1670 \text{ cm}^{-1}$ and $g = 0.9$.

$\alpha_\lambda \text{ (cm}^{-1}\text{)}$	ω_λ	R	T
0.0000	1.00000000	0.9899	0.0101
0.0001	0.99999994	0.9898	0.0100
0.0010	0.99999940	0.9883	0.0093
0.0050	0.99999701	0.9827	0.0068
0.0070	0.99999581	0.9803	0.0059
0.0100	0.99999401	0.9770	0.0048
0.1000	0.99994012	0.9307	0.0001

should indeed be less than 0.01 cm^{-1} (referring to Table 2). The uncertainty in the integrating sphere measurement for the 10-mm-thick sample is large due to the low signal-to-noise ratio. The uncertainty associated with the integrating sphere measurements for most samples is greater than that in the scatterometer measurement. Therefore, the integration of BRDF and BTDF allows a more accurate determination of R and T at the laser wavelength. Because the obtained a_λ is at least four orders of magnitude smaller than the scattering coefficient, the absorption in PTFE films is neglected hereafter. It should be mentioned that the absorption coefficient of PTFE is much smaller than typical biological tissues.

If the collimated light transmittance T_d is significant, the scattering coefficient can easily be determined by using Beer's law $T_d = \exp(-\sigma_\lambda d)$. For highly scattering samples, however, the optical signal received by the detector when $\theta_o = \theta_i$ contains both the collimated light transmitted through the sample without scattering and the scattered light. The correct way to determine T_d is to subtract the power received by the detector at $\theta_o = 0$ deg for normal incidence to that at $\theta_o = \delta$, where δ is a small angle from 1 to 3 deg that allows the detector to stay away from direct light exposure. Unfortunately, even for the thinnest sample in this study, no peaks in the BTDF can be observed around $\theta_o = 0$ deg. The BTDF of sample 1 (109 μm thick) for eight different measurements at normal incidence are plotted in Fig. 7 for $\theta_o = 0$ to 6 deg with a 1-deg interval. The fitted curve and the error bounds with 95% confidence interval are also shown. The resulting BTDF is rather flat in this region and no peak can be seen at $\theta_o = 0$ deg, suggesting that the transmitted collimated light is overwhelmed by the scattered light in the direction parallel to the incidence. In other words, the contribution of the collimated light transmission to the BTDF must be less than the uncertainty, which is about $\Delta f = 0.012 \text{ sr}^{-1}$ at the 95% confidence level. Therefore, the maximum direct transmittance (transmitted power divided by the incident laser power) should be $\Delta f \delta \Omega_o = 2.2 \times 10^{-6}$. Setting $T_d = \exp(-\sigma_\lambda d) = 2.2 \times 10^{-6}$ yields $\sigma_\lambda \approx 1200 \text{ cm}^{-1}$, which may be regarded as the lower limit of the scattering coefficient. If the scattering coefficient were less than $\sigma_\lambda \approx 1200 \text{ cm}^{-1}$, a distinguishable peak, exceeding the upper bound of the uncer-

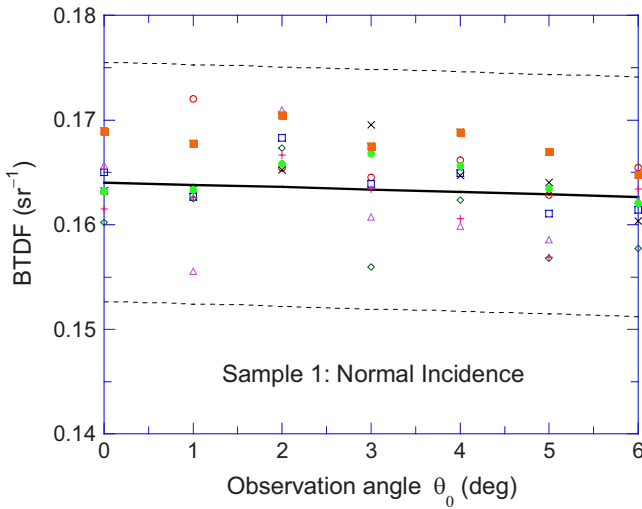


Fig. 7 BTDF of sample 1 at normal incidence for eight measurements in the observation angle range from 0 to 6 deg. The solid line represents the quadratic fit of the average BTDF, discussed previously in Fig. 3, whereas the dashed lines denote the uncertainty bounds with 95% confidence interval.

tainty, would have appeared in the BTDF at $\theta_o=0$ deg.

Under the condition that the wave-like interactions and the dependent scattering are negligible, the mean free path should be greater than several wavelengths. Suppose that the minimum mean free path is $2.5 \mu\text{m}$, which is approximately four times the laser wavelength (i.e., 635 nm), then the upper limit of the scattering coefficient is estimated to be 4000 cm^{-1} . Based on $\sigma_\lambda(1-g)=\sigma'_\lambda=167 \text{ cm}^{-1}$ and $1200 \text{ cm}^{-1} < \sigma_\lambda < 4000 \text{ cm}^{-1}$, the asymmetric parameter g should be between 0.86 and 0.96, suggesting that PTFE is a strongly forward scattering material. Compared with the parameters of biological tissues, the scattering coefficient of PTFE is approximately ten times larger.¹⁷ Much thinner samples, e.g., $d < 30 \mu\text{m}$, would be necessary to precisely determine the scattering coefficient of PTFE.

3.3 Monte Carlo Simulation

The purpose of using Monte Carlo simulation is to see how volume scattering affects the BRDF and BTDF, without considering surface scattering and polarization effects. In the calculation, the parameters are set to be $\sigma'_\lambda=167 \text{ cm}^{-1}$ and $g=0.9$, i.e., $\sigma_\lambda=1670 \text{ cm}^{-1}$. The simulation results of BRDF and BTDF at normal incidence are shown in Fig. 8. Compared with the measurements shown in Fig. 2, the Monte Carlo simulation can predict the general trend of the BRDF but with a rapid drop at large observation angles. The Monte Carlo results do not show the hump near $\theta_o=0$ deg, because the hump is associated with the surface scattering effect. Note that the humps are more prominent for samples 1 to 3 than for samples 4 and 5. It should be noted that the Monte Carlo model predicted the same R and T as the adding-doubling method did. For the BTDF, the Monte Carlo simulation also captures the essential features qualitatively; but the resulting BTDF exhibits a much larger angular variation compared with the experimental results. There are two reasons for this discrepancy. First, if surface scattering were included, there will

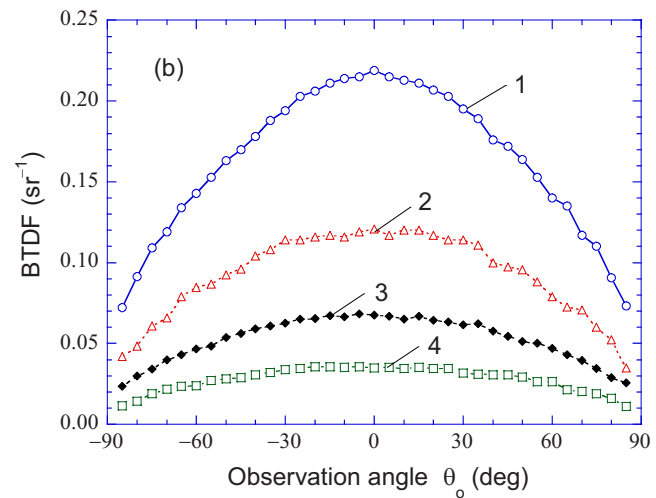
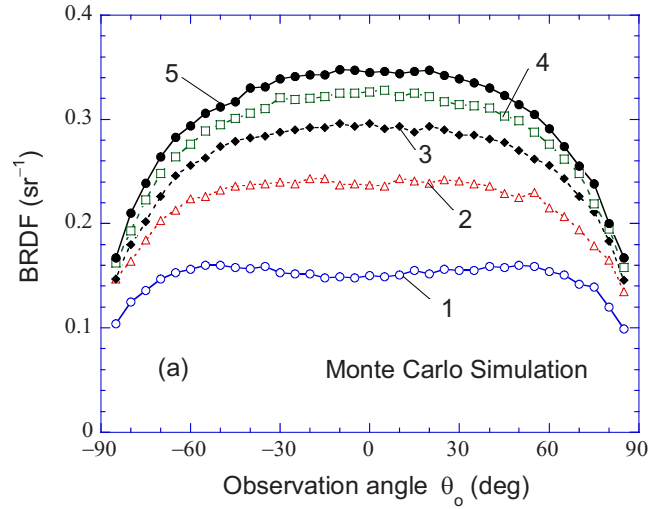


Fig. 8 Monte Carlo simulation of (a) BRDF and (b) BTDF at normal incidence.

be a total internal reflection for light emerged from PTFE to air at polar angles (inside PTFE) greater than the critical angle $\theta_c=\sin^{-1}(1/n)\approx 47$ deg. This critical angle may largely affect the energy distribution at large observation angles. Second, the Henyey–Greenstein scattering phase function is an oversimplified one, and its applicability for predicting the bidirectional scattering properties may be questionable.

Figure 9 shows the cosine θ_o modified BRDF and BTDF for sample 2 at oblique incidence. Even without considering polarization dependence and surface scattering, the BRDFs exhibit asymmetric characteristics due to the enhanced forward scattering and reduced backward scattering at increase incidence angles, although the enhancement and reduction are overpredicted in the Monte Carlo simulation. Furthermore, the Monte Carlo simulation cannot capture the specular peaks for s -polarization as observed experimentally. For BTDF, the Monte Carlo simulation predicts the symmetric feature with respect to $\theta_o=0$ deg, but overpredicts the reduction of BTDF at large incidence angles. Future research is needed to develop a more sophisticated Monte Carlo model to include surface reflection and refraction by considering the surface roughness and polarization dependence.

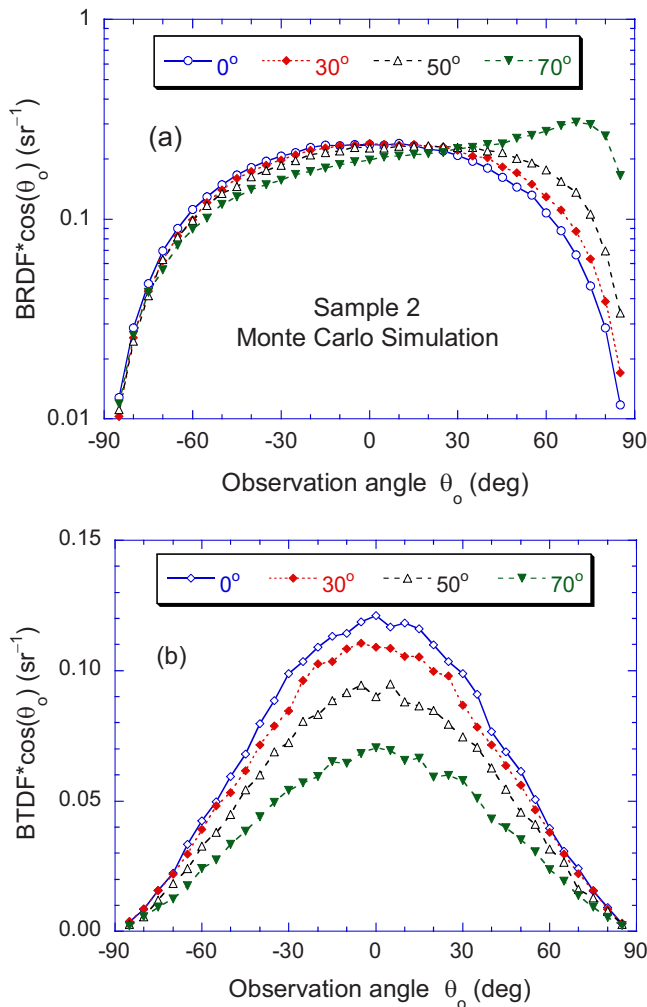


Fig. 9 Monte Carlo simulation of the (a) BRDF and (b) BTDF of sample 2 at different incidence angles.

3.4 Spectral Reflectance and Transmittance Measurements

The directional-hemispherical reflectance and transmittance of the PTFE films were measured using the system of monochromator and integrating sphere as discussed previously. Care must be taken for the transmittance measurement. The reference signal is obtained by sending the light directly to the back of the sphere. On the other hand, when the sample covers the front entrance port, the transmitted light is diffuse. For the reflectance measurement, sample 5 is used as the reference and it is placed on the back port of the sphere facing the laser. The other samples are interchanged to obtain the ratio of the reflected signal. It is assumed that the reflectance of the 10-mm-thick PTFE sample is 0.988, as determined by integration of the BRDF. The results of R and T obtained by integrating BRDF and BTDF are shown as square marks. The measured R and T using the diode laser at 635 nm with the sphere are shown with the diamond marks. All the measured results agree very well. The relative uncertainty of the reflectance and transmittance measurements was estimated to be 10% with a confidence level of 95%.

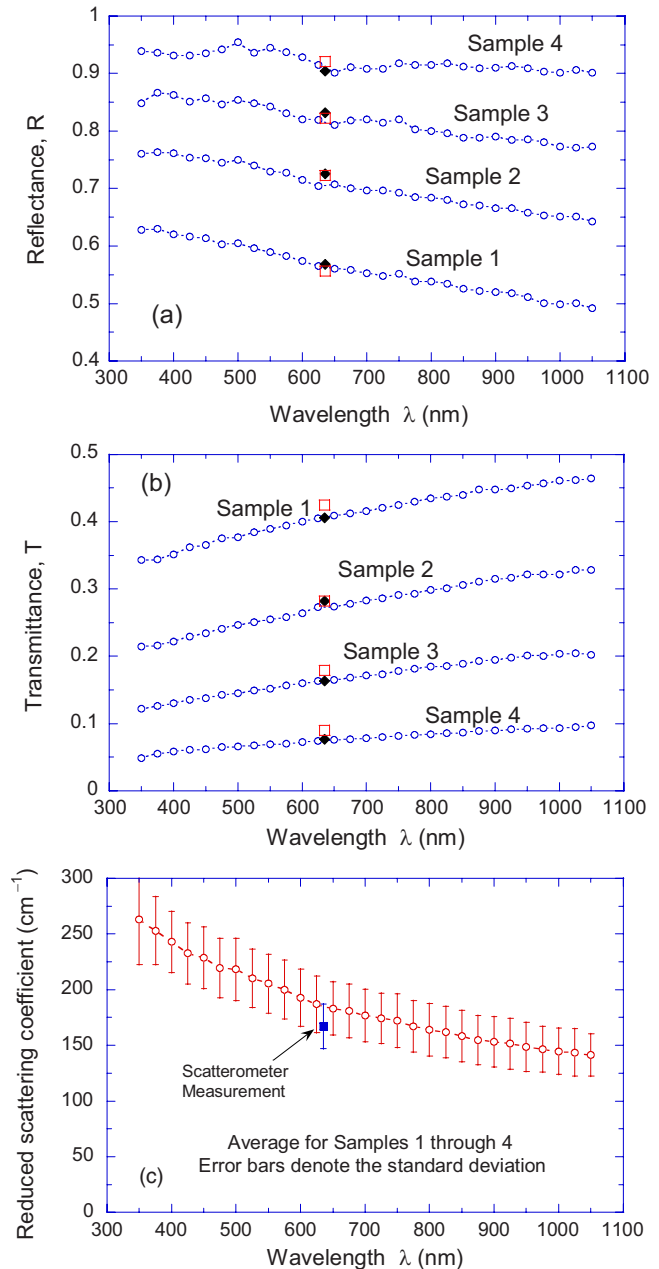


Fig. 10 Spectral, directional-hemispherical (a) reflectance and (b) transmittance of the thin-film samples measured with an integrating sphere at normal incidence. The square marks represent data integrated from the scatterometer measurements; diamond marks represent data obtained with the diode laser at 635-nm wavelength and the integrating sphere. (c) Reduced scattering coefficient calculated from R/T , as compared with that obtained previously from the scatterometer measurements.

Figures 10(a) and 10(b) show the measured spectral reflectance and transmittance in the wavelength region from 350 to 1050 nm of samples 1 to 4. As the thickness decreases, the transmittance increases but the reflectance decreases. As the wavelength increases, the reflectance decreases but the transmittance increases. This suggests that the scattering is stronger toward short wavelengths, as expected for small particle scattering. The reduced scattering coefficient

cient can be calculated using the formula $R/T=0.59\sigma'_\lambda d$ for each sample at each measurement wavelength. The average σ'_λ for the four samples and its standard deviation are plotted in Fig. 10(c). It can be clearly seen that the reduced scattering coefficient increases as the wavelength is reduced. Furthermore, the value obtained previously with the scatterometer measurement of $\sigma'_\lambda=167\text{ cm}^{-1}$ at $\lambda=635\text{ nm}$ is slightly lower than that obtained with the integrating sphere; but the agreement is within the expanded uncertainty.

4 Conclusions

A comprehensive experimental study is performed for a set of sintered PTFE films that are semitransparent and scatter light volumetrically. The BRDF and BTDF are obtained at the wavelength of 635 nm with a laser scatterometer at various angles of incidence for both polarizations. Integrating the BRDF and BTDF in the hemisphere results in directional-hemispherical reflectance and transmittance, respectively. Analyzing the reflectance-to-transmittance ratio allows the determination of a reduced scattering coefficient $\sigma'_\lambda=167\text{ cm}^{-1}$. The scattering coefficient σ_λ cannot be easily determined because the collimated light transmission is negligible, even for the thinnest sample studied here. An effort is made to estimate the range of σ_λ to be between 1200 and 4000 cm^{-1} . The absorption coefficient is estimated to be less than 0.01 cm^{-1} . Furthermore, the effect of wavelength is investigated measuring R and T in the region from 350 to 1050 nm.

Contrary to previously reported scattering coefficient and absorption coefficients of PTFE being similar to those of biological tissues, this study reveals that the scattering coefficient of PTFE is nearly ten times greater than that of typical tissues, while the absorption coefficient of PTFE is much less. The present study calls for careful distinction between directly transmitted light and scattered light toward the direction parallel to the incidence. This is important for future research of light scattering in biological media for disease diagnostics and laser therapy.

A Monte Carlo simulation is performed without considering surface scattering and polarization effects. Some of the features in the BRDF and BTDF cannot be described by the simple Monte Carlo model, suggesting the need to develop more comprehensive theoretical models that can include scattering by rough surfaces as well as volume scattering. The polarization-dependent BRDF and BTDF data presented in this work will be useful for model validation. The microstructure of PTFE depends on crystallization, particle cluster size, porosity, density, etc. Further study is also needed to investigate the effect of microstructures on the interaction of light with PTFE and other scattering materials.

Acknowledgments

The authors thank S. A. Prahl at Oregon Health and Science University for the communication on the adding-doubling software. Authors Lee and Zhang acknowledge the support of the National Science Foundation (CBET-0500113), and Zhang also acknowledges the support of the Department of Energy (DE-FG02-06ER46343) and the Optical Technology Division of NIST. Certain commercial equipment, instruments, or materials are identified in this work to foster understanding. Such identification does not imply recommendation or endorsement

by the National Institute of Standards and Technology, nor does it imply that the materials or equipment identified are necessarily the best available for the purpose.

References

1. V. R. Weidner, J. J. Hsia, and B. Adams, "Laboratory intercomparison study of pressed polytetrafluoroethylene powder reflectance standards," *Appl. Opt.* **24**(14), 2225–2230 (1985).
2. C. J. Bruegge, A. E. Stiegman, R. A. Rainen, and A. W. Springsteen, "Use of spectralon as a diffuse reflectance standard for in-flight calibration of earth-orbiting sensors," *Opt. Eng.* **32**(4), 805–814 (1993).
3. G. B. Courreges-Lacoste, J. G. Schaarsberg, R. Sprik, and S. Delwart, "Modeling of Spectralon diffusers for radiometric calibration in remote sensing," *Opt. Eng.* **42**(12), 3600–3607 (2003).
4. B. T. McGuckin, D. A. Haner, and R. T. Menzies, "Multiangle imaging spectroradiometer: optical characterization of the calibration panels," *Appl. Opt.* **36**(27), 7016–7022 (1997).
5. A. E. Stiegman, C. J. Bruegge, and A. W. Springsteen, "Ultraviolet stability and contamination analysis of Spectralon diffuse reflectance material," *Opt. Eng.* **32**(4), 799–804 (1993).
6. M. D. Fairchild and D. J. O. Daoust, "Goniospectrophotometric analysis of pressed PTFE powder for use as a primary transfer standard," *Appl. Opt.* **27**(16), 3392–3396 (1988).
7. C. S. Kim and H. J. Kong, "Rapid absolute diffuse spectral reflectance factor measurements using a silicon-photodiode array," *Color Res. Appl.* **22**(4), 275–279 (1997).
8. V. R. Weidner and J. J. Hsia, "Reflection properties of pressed polytetrafluoroethylene powder," *J. Opt. Soc. Am.* **71**(7), 856–861 (1981).
9. A. Sadhwani, K. T. Schomacker, G. J. Tearney, and N. S. Nishioka, "Determination of Teflon thickness with laser speckle. 1. Potential for burn depth diagnosis," *Appl. Opt.* **35**(28), 5727–5735 (1996).
10. S. Chandrasekhar, *Radiative Transfer*, Dover, New York (1960).
11. K. Stamnes, S.-C. Tsay, W. Wiscombe, and K. Jayaweera, "Numerically stable algorithm for discrete-ordinate-method radiative transfer in multiple scattering and emitting layered media," *Appl. Opt.* **27**(12), 2502–2509 (1988).
12. A. Ambirajan and D. C. Look Jr., "A backward Monte Carlo estimator for the multiple scattering of a narrow light beam," *J. Quant. Spectrosc. Radiat. Transf.* **56**(3), 317–336 (1996).
13. K. I. Gjerstad, J. J. Stamnes, B. Hamre, J. K. Lotsberg, B. Yan, and K. Stamnes, "Monte Carlo and discrete-ordinate simulations of irradiances in the coupled atmosphere-ocean system," *Appl. Opt.* **42**(15), 2609–2622 (2003).
14. J. R. Howell, "The Monte Carlo method in radiative heat transfer," *J. Heat Transfer* **120**(3), 547–560 (1998).
15. L. Roberti, "Monte Carlo radiative transfer in the microwave and in the visible: biasing techniques," *Appl. Opt.* **36**(30), 7929–7938 (1997).
16. S. A. Prahl, "Light transport in tissue," PhD dissertation, Univ. of Texas at Austin (1988).
17. W. F. Cheong, S. A. Prahl, and A. J. Welch, "A review of the optical properties of biological tissues," *IEEE J. Quantum Electron.* **26**(12), 2166–2185 (1990).
18. J. W. Pickering, S. A. Prahl, N. van Wieringen, J. F. Beek, H. J. C. M. Sterenborg, and J. C. van Gemert, "Double-integrating-sphere system for measuring the optical properties of tissue," *Appl. Opt.* **32**(4), 399–410 (1993).
19. D. Zhu, W. Lu, S. Zeng, and Q. Luo, "Effect of light losses of sample between two integrating spheres on optical properties estimation," *J. Biomed. Opt.* **12**(6), 064004 (2007).
20. S. A. Prahl, M. J. C. van Gemert, and A. J. Welch, "Determining the optical properties of turbid media by using the adding-doubling method," *Appl. Opt.* **32**(4), 559–568 (1993).
21. D. K. Sardar, M. L. Mayo, and R. D. Glickman, "Optical characterization of melanin," *J. Biomed. Opt.* **6**(4), 404–411 (2001).
22. N. Huber, J. Heitz, and D. Bauerle, "Pulsed-laser ablation of polytetrafluoroethylene (PTFE) at various wavelengths," *Eur. Phys. J.: Appl. Phys.* **25**, 33–38 (2004).
23. Y. J. Shen, Q. Z. Zhu, and Z. M. Zhang, "A scatterometer for measuring the bidirectional reflectance and transmittance of semiconductor wafers with rough surfaces," *Rev. Sci. Instrum.* **74**(11), 4885–4892 (2003).
24. H. J. Lee, A. C. Bryson, and Z. M. Zhang, "Measurement and modeling of the emittance of silicon wafers with anisotropic roughness,"

- Intl. J. Thermophys.* **28**, 918–932 (2007).
25. H. C. van de Hulst, *Multiple Light Scattering*, Vol. 1, Academic Press, New York (1980).
 26. W. H. Press, B. P. Flannery, S. A. Teukolsky, and W. T. Vetterling, *Numerical Recipes in C*, Cambridge University Press, New York (2002).
 27. L. Wang, S. L. Jacques, and L. Zheng, “MCML—Monte Carlo modeling of light transport in multi-layered tissues,” *Comput. Methods Programs Biomed.* **47**(2), 131–146 (1995).
 28. E. A. Early, P. Y. Barnes, B. C. Johnson, J. J. Butler, C. J. Bruegge, S. F. Biggar, P. R. Spyak, and M. M. Pavlov, “Bidirectional reflectance round-robin in support of the Earth Observing System program,” *J. Atmos. Ocean. Technol.* **17**, 1077–1091 (2000).
 29. P. Kubelka, “New contributions to the optics of intensely light-scattering materials. Part I,” *J. Opt. Soc. Am.* **38**(5), 448–457 (1948).
 30. P. S. Mudgett and L. W. Richards, “Multiple scattering calculations for technology,” *Appl. Opt.* **10**(7), 1485–1502 (1971).
 31. W. M. Star, J. P. A. Marijnissen, and M. J. C. van Gemert, “Light dosimetry in optical phantoms and in tissues: I. Multiple flux and transport theory,” *Phys. Med. Biol.* **33**(4), 437–454 (1988).